DIFFERENCE IMAGE OF SEISMIC REFLECTION SECTIONS WITH HIGHLY DENSE SPATIAL SAMPLING IN RANDOM HETEROGENEOUS MEDIA

JUN MATSUSHIMA[1] and OSAMU NISHIZAWA[2]

[1] *School of Engineering, The University of Tokyo, Toyo, Japan. jun-matsushima@frcer.t.u-tokyo.ac.jp*
[2] *Geological Survey of Japan, AIST, Tokyo, Japan.*

(Received January 10, 2010; revised version accepted May 7, 2010)

ABSTRACT

Matsushima, J. and Nishizawa, O., 2010. Difference image of seismic reflection sections with highly dense spatial sampling in random heterogeneous media. *Journal of Seismic Exploration*, 19: 279-301.

According to the Nyquist sampling criterion, it is redundant to deploy a smaller sampling interval than the Nyquist sampling interval. However, we show the possibility of utilizing a highly dense deployment of source/receivers when applying seismic reflection methods in random heterogeneous media. We consider a seismic waveform consisting of scattered waves generated by random isotropic heterogeneity, which is a noise-like wave field caused by multiple scattering of seismic waves. The final section contains disturbance due to the multiple-scattering effects in small-scale heterogeneities that do not satisfy the assumption of migration theory based on single scattering. Our numerical experiments indicate that the highly dense spatial sampling does not improve resolution of the section when the subsurface structure contains random heterogeneity regardless of the relationship between the spatial sampling interval and the characteristic size of heterogeneities, even if the interval of spatial sampling becomes shorter than the Nyquist sampling interval. However, we found the existence of a small but significant difference between two sections generated with adequate sampling. This small but significant difference is attributed to both the truncation artifact and NMO-stretch effect which cannot be practically prevented during data acquisition and processing. We show that this small difference is dependent on the characteristic heterogeneity size, indicating that difference images have the possibility of estimating the characteristic size of heterogeneities by differentiating two sections with different adequate spatial sampling.

KEYWORDS: Nyquist sampling theorem, difference image, spatial sampling, random heterogeneous media, scattering, NMO-stretch effect, truncation artifact, aliasing, time-lapse.

0963-0651/10/$5.00

INTRODUCTION

In most reflection seismic explorations, it is implicitly assumed that the subsurface target heterogeneities are so large and strong that other background heterogeneities cause only small fluctuations in signals from the target. In this case, a clear distinction can be made between target structures and the small-scale background heterogeneities. However, complicated waveforms appear if the small-scale heterogeneities are significantly strong and are of comparable size to the seismic wavelength. This complication makes investigating subsurface structures difficult. In deep crustal studies (Brown et al., 1983) or geothermal studies (Matsushima et al., 2003), seismic data often have a poor signal-to-noise ratio. Complicated seismic waves are due to seismic wave scattering generated from the small-scale heterogeneities, which degrades seismic reflection data, resulting in attenuation and travel time fluctuations of reflected waves, and the masking of reflected waves by multiple scattering events. In this case, the conventional single-scattering assumption of migration may not be applicable; in other words, multiple scattering caused by strong heterogeneities may disturb the energy distribution in observed seismic traces (Emmerich et al., 1993).

The understanding of seismic wave propagation in random heterogeneous media has been well advanced by many authors on the basis of theoretical studies (Sato and Fehler, 1998), numerical studies (Frankel and Clayton, 1986; Hoshiba, 2000), and experimental studies (Nishizawa et al., 1997; Sivaji et al., 2001). Since scattered waves are incoherent and the small-scale heterogeneity is presumed to be randomly distributed, the statistical properties of seismic wave fluctuation relate to the statistical properties of this small-scale heterogeneity. Seismologists conclude that coda waves are one of the most convincing pieces of evidence for the presence of random heterogeneities in the Earth's interior. Seismic evidence suggests random heterogeneity on a scale ranging from tens of meters to tens of kilometers. In addition, geologic studies of exposed deep crustal rocks indicate petrologic variations in the lithosphere on a scale of meters to kilometers (Karson et al., 1984). Well-logging data suggest that small-scale heterogeneities have a continuous spectrum (Shiomi, 1997).

Wave phenomena in heterogeneous media are important for seismic data processing but have not been well recognized and investigated in the field of seismic exploration. Numerical studies by Gibson and Levander (1988) indicate that different types of scattered noise can have different effects on the appearance of the final processed section. Gibson and Levander (1990) showed the apparent layering in CMP sections of heterogeneous targets. Emmerich et al. (1993) also concluded that the highly detailed interpretation, which is popular in crustal reflection seismology, is less reliable than believed, as far as the internal structure of scattering zones and scatterer orientations are concerned.

Sick et al. (2003) proposed a method that compensates for the scattering attenuation effects from random isomorphic heterogeneities to obtain a more reliable estimation of reflection coefficients for AVO/AVA analysis. It is important to understand how scattered waves caused by random heterogeneities affect data processing in seismic reflection studies and how these effects are compensated for.

A primary concern of this article is to study the effect of spatial sampling on the images of seismic reflection in random heterogeneous media. According to the Nyquist sampling criterion, it is redundant to deploy sampling intervals smaller than the Nyquist sampling interval. However, we investigate the relationship between the spatial sampling interval and the characteristic size of heterogeneities and also investigate from the viewpoint of spatial sampling how noise-like scattered wave fields that are produced from random isotropic heterogeneity influence the seismic section. We consider the adoption of highly dense spatial sampling with intervals smaller than the Nyquist interval to improve the final quality of a section. Although migration techniques generally assume that the seismic data to be migrated consists only of primary reflections and diffractions, migration fails to image random heterogeneities due to multiple-scattering effects in small-scale heterogeneities that do not satisfy the assumption of migration theory based on single scattering. In this paper, conventional poststack migration is performed to examine different responses to the migration effect of different spatial sampling intervals. We generate 2D finite-difference synthetic seismic data as input to this study. Our numerical models have a horizontal layered structure, upon which randomly distributed heterogeneities are imposed.

PROPER SPATIAL SAMPLING INTERVAL IN SEISMIC REFLECTION

According to the Nyquist sampling theorem, sampling at two points per wavelength is the minimum requirement for sampling seismic data over the time and space domains; that is, the sampling interval in each domain must be equal to or above twice the highest frequency/wavenumber of the continuous seismic signal being discretized. The phenomenon that occurs as a result of undersampling is known as aliasing. Aliasing occurs when recorded seismic data violate the criterion expressed in eq. (1).

$$\Delta x \leq \Delta x_N = v_{min}/(2f_{max}\cdot\sin\theta) \quad , \tag{1}$$

where Δx is the spatial sampling interval which should be equal to or smaller than the spatial Nyquist sampling intervals Δx_N, v_{min} is the minimum velocity, f_{max} is the maximum frequency, and θ is the dip angle of the incident plane-wave direction.

On the other hand, in the case of zero-offset, the spatial sample interval should be equal to or smaller than a quarter-wavelength (Grasmueck et al., 2005). Yilmaz (1987) described that aliasing occurs when recorded seismic data violate the criterion expressed in eq. (2),

$$\Delta x \leq \Delta x_N = v_{min}/(4f_{max}\cdot\sin\theta) \quad . \tag{2}$$

In the presence of structural dips or significant lateral velocity variations, adequate sampling becomes important for both vertical and lateral resolution. For the case of the maximum dip ($\theta = 90°$), the spatial Nyquist sampling interval becomes a quarter-wavelength. Thus, quarter-wavelength spatial sampling is a minimum requirement for adequate recording. Vermeer (1990) defined the term "full-resolution recording" for unaliased shooting and recording of the seismic wave field at the basic signal-sampling interval. In practice, however, seismic data are often irregularly and/or sparsely sampled in the space domain because of limitations such as those resulting from difficult topography or a lack of resources. In many cases, proper sampling is outright impossible. In order to avoid aliasing, standard seismic imaging methods discard some of the high frequency components of recorded signals. Valuable image resolution will be lost through processing seismic data (Biondi, 2001). Once seismic data are recorded, it is difficult to suppress aliasing artifacts without resurveying at a finer spatial sampling (Spitz, 1991). On the other hand, note that the estimation of seismic wave attenuation (or velocity) using a vertical seismic profile (VSP) is free from the Nyquist sampling theorem, that is, the smaller spatial sampling can capture the wave field of smaller heterogeneities (e.g., Maresh et al., 2006).

In the case of migration processing, there are three types of aliasing (Biondi, 2001), associated with data, operator, and image spacing. Data space aliasing is the aliasing described above. Operator aliasing, which is common in Kirchhoff migration algorithms, occurs when the migration operator summation trajectory is too steep for a given input seismic trace spacing and frequency content. Kirchhoff migration approximates an integral with a summation and is subject to migration operator aliasing when trace spacings do not support the dip of the migration operator. In contrast, migration algorithms such as the f-k method or finite-difference methods only require that the input data volume be sampled well enough to avoid aliasing of the input volume (Abma et al., 1999). Adequate solution for operator aliasing is to control the frequency content (e.g., low-pass filtering at steep dips). The anti-aliasing constraints to avoid operator aliasing can be easily derived from the Nyquist sampling theorem. The resulting anti-aliasing constraints are (Biondi, 1998):

$$f \leq 1/(2\Delta x_{data}\cdot p_{op}) \quad , \tag{3}$$

where Δx_{data} is the sampling rate of the data x-axis and p_{op} is the operator dip.

Image space aliasing occurs when the spatial sampling of the image is too coarse to adequately represent the steeply dipping reflectors that the imaging operator attempts to build during the imaging process. Image space aliasing can be avoided simply by narrowing the image interval. But for a given spatial sampling of the image, to avoid image space aliasing we need to control the frequency content of the image. Similarly to the case of operator aliasing, the anti-aliasing constraints to avoid image space aliasing can be easily derived from the Nyquist sampling theorem. The resulting anti-aliasing constraints are (Biondi, 1998):

$$f \leq 1/(2\Delta x_{image} \cdot p_{ref}) \quad , \tag{4}$$

where Δx_{image} is the image sampling rate of the x-axis; p_{ref} is the reflector dip.

NUMERICAL SIMULATIONS

We constructed a synthetic seismic data set propagating through two-dimensional random heterogeneous media where random velocity variation was superimposed on a two-layer model. The random heterogeneity generated incoherent events by scattering of waves that contained reflection events. The synthetic data were generated with a second-order finite difference scheme for the constant density two-dimensional acoustic wave equation. In the following, we describe the method for creating models and for calculating the wave field.

To minimize grid dispersion in finite difference modeling, the grid size was set to be about one eighteenth of the shortest wavelength, which was calculated from the minimum velocity of 3600 m/s, the maximum frequency of around 40 Hz (f_{max} = 40), and a 5-m grid spacing. All edges of the finite-difference grid were set to be far from source/receiver locations so that unnecessary events would not disturb the synthetic data. Source/receivers were not located on the edge of the model, but within the model body. In this situation, scattered wave fields generated in the heterogeneous media above the source/receiver locations would be included in the synthetic data. However, this does not affect the conclusions of this article.

Layered model overlapped with random heterogeneity

Random heterogeneous media are generally described by fluctuations of wave velocity and density, superposed on a homogeneous background. Their properties are given by an autocorrelation function parameterized by the correlation lengths and the standard deviation of the fluctuation. Random media with spatial variations of seismic velocity were generated by the same method as described in Frankel and Clayton (1986). The outline of the scheme is as

follows:

1. Assign a velocity value v(x,z) to each grid point using a random number generator.

2. Fourier transform the velocity map into the wave number space.

3. Apply the desired filter in the wavenumber domain.

4. Fourier transform the filtered data back into the spatial domain.

5. Normalize the velocities by their standard deviation, centered on the mean velocity.

In this paper, the applied filter (Fourier transform of autocorrelation function, which is equal to the power spectral density function) has a von Karman probability distribution described by eq. (5):

$$P(k,a) = 4\pi\beta a^2/(1 + k^2a^2)^{\beta+1} \quad , \tag{5}$$

where k is the wavenumber, β is the Hurst number that controls the components of small scale random heterogeneities, and a is the correlation distance indicating the characteristic heterogeneity size. The wavenumber k we use here is defined by eq. (6):

$$k = 2\pi/\lambda \quad , \tag{6}$$

where λ is the wavelength. We use the above von Karman-type heterogeneous media with $\beta = 0.1$. Saito et al. (2003) described that the value $\beta = 0.1$ is nearly the same as the value for the power spectral density function of velocity fluctuation obtained from well-log data at depths shallower than 10 km (e.g., Shiomi et al., 1997; Goff and Holliger, 2000).

A homogeneous model and source/receiver arrangements are shown in Fig. 1a. A reflector is placed at a depth of 2000 m, separating two layers having constant velocities of 3800 m/s and 4200 m/s, respectively. Three different source-receiver intervals of width 5, 20, and 80 m were employed; each requiring 401, 101, and 26 sources and receivers, respectively. To estimate the relationship between the spatial sampling interval and the characteristic size of heterogeneities, two types of random heterogeneities were generated and implemented in the layered model as shown in Fig. 1b. The velocity perturbations shown in Fig. 1b were normalized to have a standard deviation 3% of the 3800 m/s (upper) and 4200 m/s (lower) layers on average and a characteristic heterogeneity size of 10 m (a = 10 m). Fig. 1c is the same as Fig. 1b except for characteristic heterogeneity sizes of 50 m (a = 50 m).

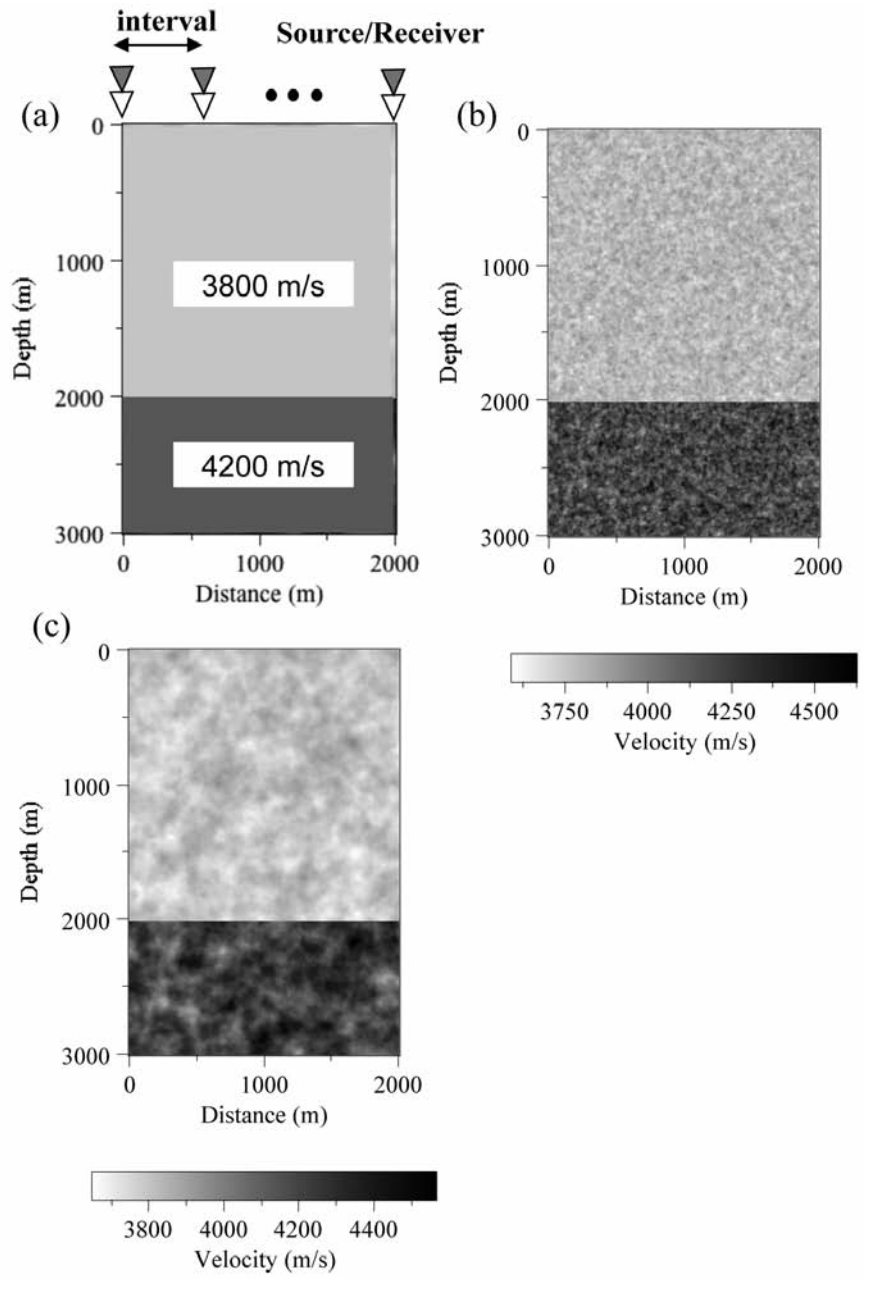

Fig. 1. (a) A single-interface model for numerical simulation examining specifications of data acquisition in reflection seismic surveys. A reflector is placed at a depth of 2000 m. (b) The first two-layered random media model for two-dimensional acoustic wave simulation using the finite-difference method. The average velocity of the upper layer is 3800 m/s with 3% standard deviation and correlation distance 10 m. (c) The second two-layered random media model with the same average velocity and standard deviation as for (b), except for a correlation distance of 50 m.

Wave field calculation

We employed a 2D finite difference method for heterogeneous media with random spatial variations in seismic velocity. The source wavelet was the Ricker wavelet with a dominant frequency of 20 Hz. The dominant frequency (20 Hz) and the average velocity (3800 m/s) yielded the dominant wavelength (190 m).

To compare results between random media of different characteristic lengths, wavelengths have to be described with reference to the characteristic lengths of random media. The product of the wavenumber k and the characteristic length a is used as an index for describing effects of random heterogeneity on seismic waves. In the present cases, the ka values at the dominant wavelengths are about 0.33 (a = 10 m) and 1.65 (a = 50 m), respectively.

Aki and Richards (1980) classified scattering phenomena in terms of two dimensionless numbers ka and kL, where L is the travel distance between source and receiver. Scattering effects are not so important for very small or very large ka, and these effects become increasingly important with increasing kL. According to this classification, our heterogeneous models are categorized as wave theories for random media where strong scattering may occur and full waveform modeling is required.

In order to remove direct wavelets, the total wave field calculated with the model shown in Figs. 1b and 1c was subtracted from the wave field in a model with a constant velocity of 3800 m/s to produce the wave field containing the reflected/scattered wave field. Figs. 2a through 2c show an example of the shot gather from the scattered wave field in the case of a = 10 m for source-receiver intervals of 5, 20, and 80 m, respectively. Similarly, Figs. 2d through 2f show an example of the shot gather from the scattered wave field in the case of a = 50 m for source-receiver intervals of 5, 20, and 80 m, respectively. Although we can clearly see the reflection event in each shot gather, the shot gathers are full of chaotic diffraction patterns originating from random heterogeneities.

The frequency-wavenumber (f-k) diagram is helpful for visualizing the sampling of a continuous wave field (Vermeer, 1990). The time window (from 0.65 to 1.05 s) including only scattered wave fields was extracted from each shot gather to calculate an f-k plot. Figs. 3a through 3c show f-k plots of the extracted shot gather from the scattered wave field in the case of a = 10 m for source-receiver intervals of 5, 20, and 80 m, respectively. Similarly, Figs. 3d through 3f show f-k plots of the extracted shot gather from the scattered wave field in the case of a = 50 m for source-receiver intervals of 5, 20, and 80 m, respectively.

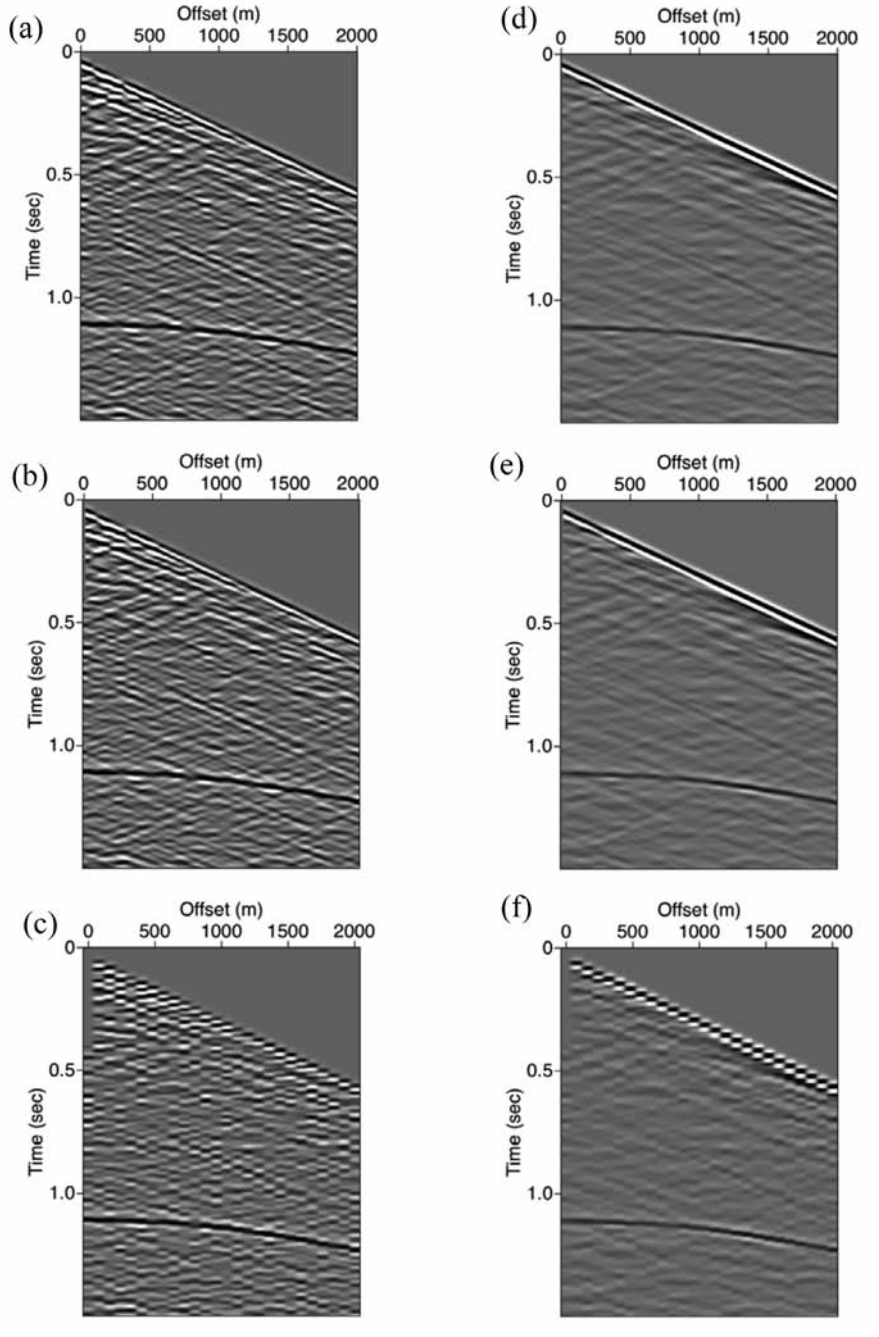

Fig. 2. Examples of common-shot gather of a scattered wave field calculated for the model with different spatial sampling intervals and characteristic heterogeneity sizes: spatial sampling intervals of (a) 5 m, (b) 20 m, and (c) 80 m for the case of for a = 10 m (Fig. 1b) and spatial sampling intervals of (d) 5 m, (e) 20 m, and (f) 80 m for the case of for a=50 m (Fig. 1c).

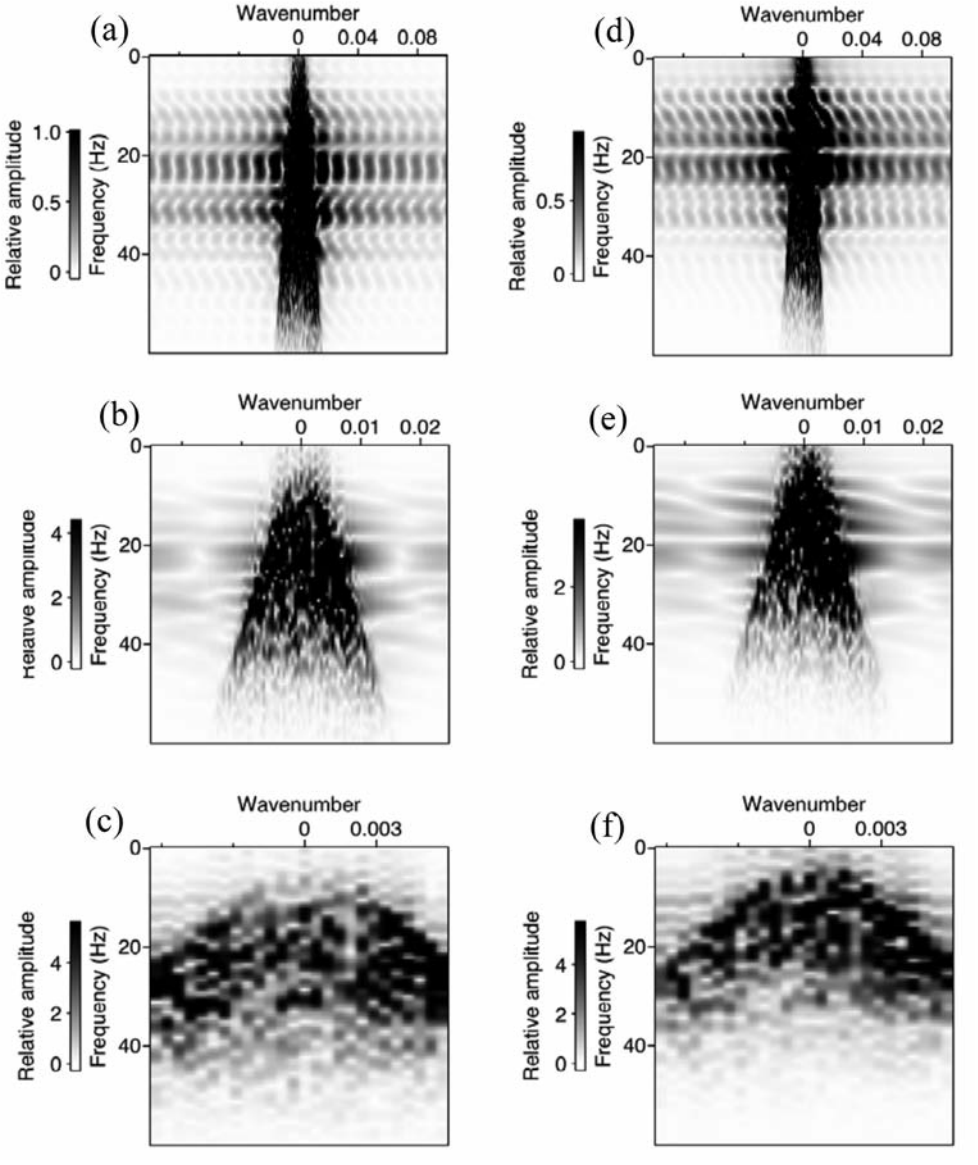

Fig. 3. Frequency-wavenumber (f-k) plots of the extracted shot gather of a scattered wave field with different spatial sampling intervals and characteristic heterogeneity sizes: spatial sampling intervals of (a) 5 m, (b) 20 m, and (c) 80 m for the case of for a = 10 m and spatial sampling intervals of (d) 5 m, (e) 20 m, and (f) 80 m for the case of for a = 50 m.

According to the spatial Nyquist sampling criterion defined in eq. (1), Δx_N becomes 45 m ($f_{max} = 40$, $v_{min} = 3600$, $\theta = 90°$). Thus, spatial sampling less than 45 m is sufficient to prevent spatial aliasing of the scattered wave field. In the case of the 80 m spatial sampling interval of Fig. 3c, the sector of strong amplitudes in the f-k plot would be severely truncated, causing wrap-around effects. On the other hand, in the case of zero-offset defined by eq. (2), spatial sampling of less than 22.5 m is sufficient to prevent spatial aliasing.

RESULTS

Poststack migrated sections

Figs. 4a through 4c show poststack migrated sections using f-k migration (Stolt, 1978) with a random heterogeneous model for the case of a characteristic heterogeneity size of 10 m (a = 10 m) with different source/receiver intervals at 5, 20, and 80 m, respectively. Similarly, Figs. 4d through 4f show poststack migrated sections for the case of a characteristic heterogeneity size of 50 m (a = 50 m) with different source/receiver intervals at 5, 20, and 80 m, respectively. In each section, we can see a reflector at around 1.1 sec. and many discontinuously subhorizontal and dipping events that partly correlate with velocity heterogeneities of the model. We can also see that numerous small segments are detectable even after the poststack migration and that the results of poststack migration for the different heterogeneous models differ with different source/receiver intervals. In general, migration can improve lateral resolution by correcting the lateral mispositioning of dipping reflectors or collapsing diffraction patterns caused by a point scatterer. However, the application of poststack migration here does not improve seismic images in heterogeneous media. It is thought that the reason is that multiple-scattering effects in small-scale heterogeneities do not satisfy the assumption of migration theory based on single scattering. Although migration techniques assume that the seismic data to be migrated consists only of primary reflections and diffractions, these wave fields are attenuated and distorted by heterogeneities and multiple scattered wave fields are generated, producing apparent discontinuities in reflectors or diffractors.

Differences between sections with different sampling intervals

Poststack migrated sections of Figs. 4a through 4c look identical in appearance. In order to examine the detailed differences between sections of Figs. 4a through 4c, the section in Fig. 4a was subtracted from those in Figs. 4b through 4c to produce the difference sections shown in Figs. 5a through 5b.

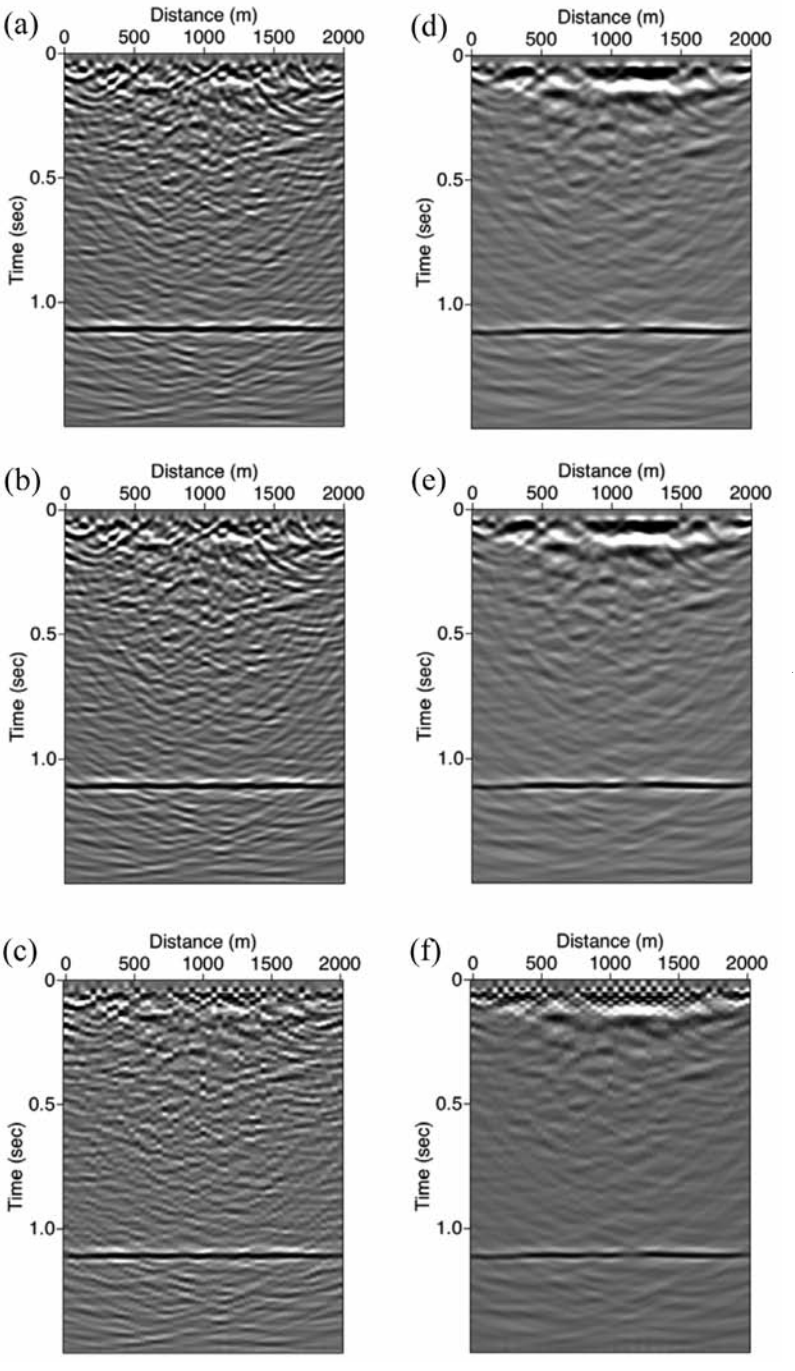

Fig. 4. Poststack migrated sections with different spatial sampling intervals and characteristic heterogeneity sizes: spatial sampling intervals of (a) 5 m, (b) 20 m, and (c) 80 m for the case of for a = 10 m and spatial sampling intervals of (d) 5 m, (e) 20 m, and (f) 80 m for the case of for a = 50 m.

Similarly, Figs. 5c through 5d show difference images between two different poststack migrated sections, as shown in Figs. 4d through 4f. During subtraction, the imaging interval of each model is set to 40 m and each section is normalized by its maximum value. Difference images show that significant differences between sections with different sampling intervals are clearly visible. Small values of differences in sections with different sampling intervals are evident. The entire appearance of the event pattern in difference images is somewhat consistent across different sampling intervals. The amplitude of difference images is increasing with increasing difference of sampling interval.

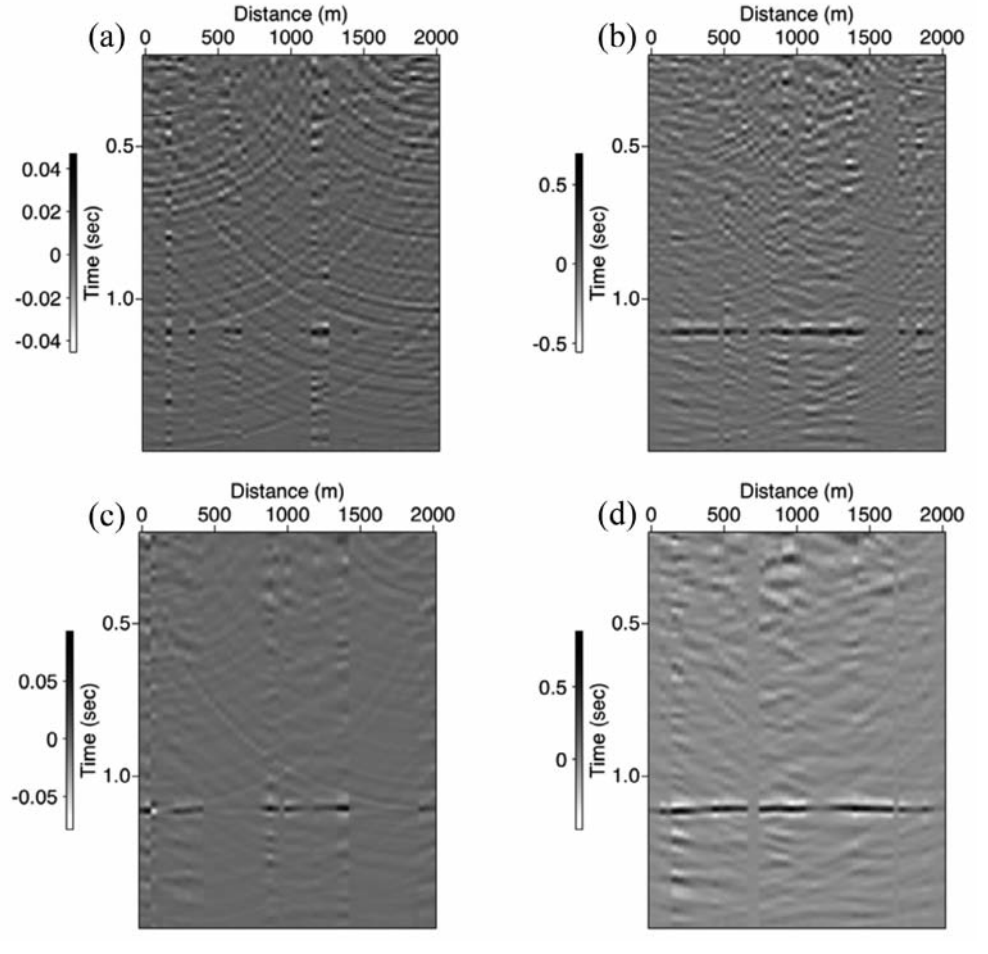

Fig. 5. Difference image of two different poststack migrated sections in the case of a = 10 m obtained by simple subtraction of (a) Fig. 4a from Fig. 4b, and (b) Fig. 4a from Fig. 4c. For the case of a = 50 m, subtraction of (c) Fig. 4d from Fig. 4e, and (d) Fig. 4d from Fig. 4f.

We can see numerous small segments and clear reflector observed at around 1.1 sec. In order to examine robustness of results, we performed the same processing with different time sampling to produce difference sections. Although the magnitude of small values of differences is different, this does not affect the conclusions of this article.

According to a close examination of the four difference images of poststack migrated sections in Fig. 5, the numerous small segments produced from scattered wave fields are dependent on the characteristic heterogeneity size. Although small-scale heterogeneities have an influence on waveform with respect to the size of heterogeneities, the scattering effect is dominant at wavelengths comparable to the scale length of heterogeneity (e.g., Nishizawa et al., 1997). Thus, the frequencies of numerous small segments produced from scattered wave fields are attributed to the difference in the size of the heterogeneities. The other feature is that the amplitude of an obscure and intermittent reflector observed at around 1.1 sec. fluctuates more with an increase in characteristic size of heterogeneity. The reason for this is due to the fluctuations in arrival times of the reflection which are attributed to differences in the size of the heterogeneities. The larger the heterogeneity size becomes, the larger the fluctuations in arrival time of the reflection become. Müller et al. (2002) observed the same phenomena using a statistical approach to describe the time-space pulse evolution in single realizations of two- and three-dimensional random media.

Relationship between characteristic size of heterogeneities and difference images

The frequency information is helpful for indicating the characteristic size of heterogeneities. The frequency-distance (f-x) domain is calculated by Fourier transform along the direction of time and averaged along the direction of distance. In the shot gathers shown in Fig. 2a and 2d, the time window (from 0.65 to 1.5 s) including both reflected and scattered wave fields was extracted to calculate an f-x domain and obtain an averaged amplitude spectrum (Fig. 6a) while the time window (from 0.65 to 1.05 s) including only scattered wave fields was extracted to calculate an f-x domain and obtain an averaged amplitude spectrum (Fig. 6b). In Figs. 6a and 6b, the solid line shows the case for a = 10 m and the dotted line shows the case for a = 50 m.

In the poststack migrated sections shown in Figs. 4a and 4d, the time window (from 0.2 to 1.5 s) including both reflected and scattered wave fields was extracted to calculate an f-x domain and obtain an averaged amplitude spectrum (Fig. 6c) while the time window (from 0.2 to 1.0 s) including only scattered wave fields was extracted to calculate an f-x domain and obtain an averaged amplitude spectrum (Fig. 6d).

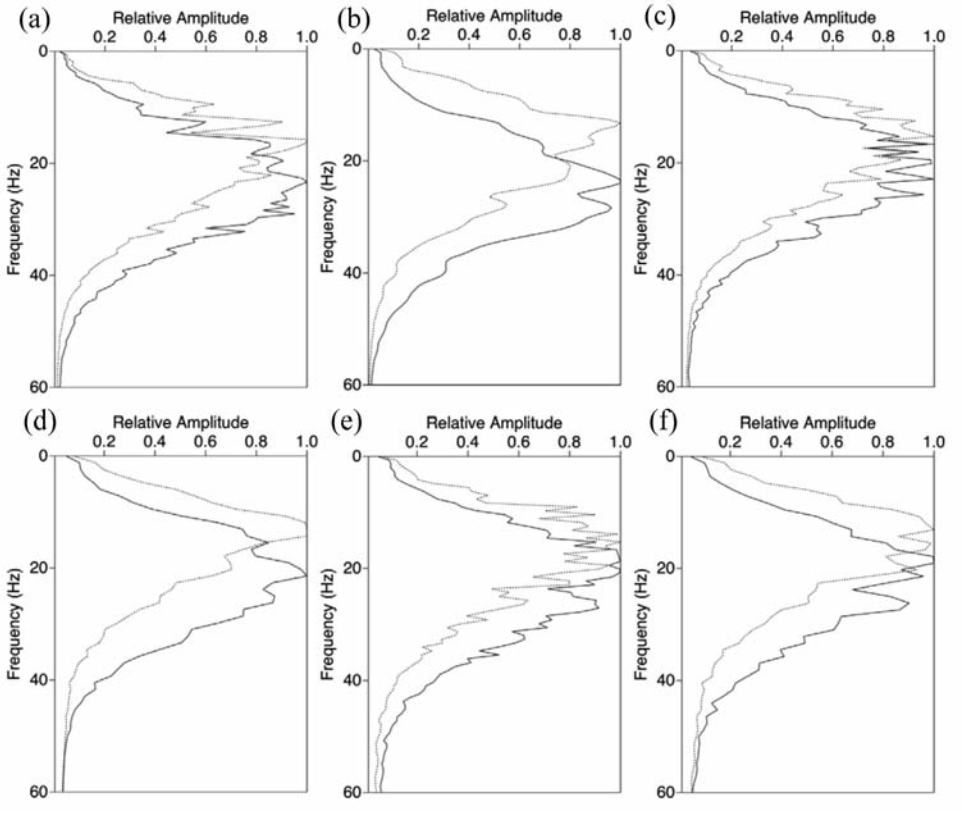

Fig. 6. Averaged amplitude spectrums for (a) shot gather including both reflected and scattered wave fields, (b) shot gather including only scattered wave fields, (c) poststack migrated section including both reflected and scattered wave fields, (d) poststack migrated section including only scattered wave fields, (e) difference images of poststack migrated section including both reflected and scattered wave fields, and (f) difference images of poststack migrated section including only scattered wave fields. In each graph, the solid line shows the case for a = 10 and the dotted line shows the case for a = 50.

In the difference images of poststack migrated sections shown in Figs. 5a and 5c, the time window (from 0.2 to 1.5 s) including both reflected and scattered wave fields was extracted to calculate an f-x domain and obtain an averaged amplitude spectrum (Fig. 6e) while the time window (from 0.2 to 1.0 s) including only scattered wave fields was extracted to calculate an f-x domain and obtain an averaged amplitude spectrum (Fig. 6f).

Finally, in Figs. 6a through 6f we can see that the averaged amplitude spectrum for a = 10 m are higher than that for a = 50 m. These systematic frequency shifts are attributable to the multiple-scattering effects in small-scale heterogeneities, that is, the smaller-scale heterogeneities generate the higher frequency wave fields. Note that such a frequency shift is observed even in the case of difference images although the magnitude of frequency shift is somewhat different. This fact indicates that difference images have the possibility of estimating the characteristic size of heterogeneities by differentiating two sections with different adequate spatial sampling. However, further investigation is needed to quantify the characteristic size of heterogeneities.

Causes of small difference between two sections

In order to examine the causes of small difference values between two sections generated with different adequate samplings, we consider the influence of two effects: truncation effect and NMO-stretch effect. We conduct simple numerical experiments. A subsurface is presumed to consist of Huygens' secondary sources, in which case imaging a subsurface is considered to be equivalent to imaging each point scatterer separately and summing the imaged point scatterers at the end.

a. *Truncation effect*

Fig. 7 shows synthetic seismic events consisting of Ricker wavelets with a central frequency of 20 Hz in the t-x plane. In Fig. 7, two kinds of events (flat and dipping) exist, with three different spatial sampling intervals (5, 20, 80 m). The dip of the dipping event is 0.3 ms/m. Here a flat event is assumed to be horizontally aligned by a NMO (Normal moveout) correction, while a dipping event is assumed to be an uncorrected reflection from a diffraction. Fig. 8 shows the transformation of the t-x domain shown in Fig. 7 into the f-k plane, illustrating that each event in t-x space corresponds to an event with a unique direction from the origin in f-k space. In the case of a spatial sampling interval of more than 40 m, we can clearly see spatial aliasing effects. Each panel of Fig. 7 is stacked horizontally to produce a stacked trace (Fig. 9). In each trace of Fig. 9, we can see a large amplitude event (indicated by Event A) at around 0.5 sec., which is generated from a flat event and other events (indicated by

Events B and C, respectively) that are generated from a dipping event.

From another viewpoint, each stacked trace generated from summing the gathers horizontally can be viewed as the interference of Ricker wavelets with different time lags (e.g., Matsushima et al., 1998). When the time lag is zero (the case of a flat event), the wavelets strengthen each other (Event A). When the time lag between wavelets is small, wavelets of a dipping event cancel each other out except at the ends of the dipping event (Event B). As the time lag between wavelets becomes much larger, the interference of the wavelets in a dipping event becomes weaker, leaving uncanceled events (Event C). The existence of Event C is due to data space aliasing, and the existence of Event B is due to the truncation artifact that is related to the finite number of traces. Furthermore, in order to examine details of the difference between traces, the section in Fig. 9a was subtracted from those in Figs. 9b through 9c to produce the difference sections shown in Figs. 10a through 10b. We can see that a large

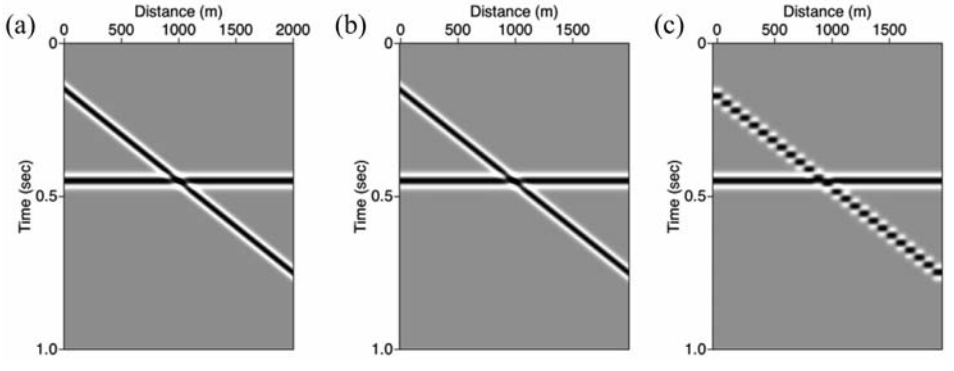

Fig. 7. Synthetic seismic gathers consisting of two different events: a flat event (dip = 0) and a dipping event (dip = 0.3 ms/m), in the t-x domain with three different spatial sampling intervals: (a) 5 m, (b) 20 m, and (c) 80 m.

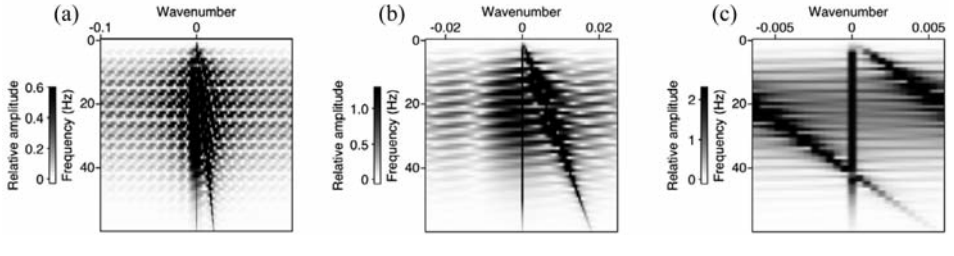

Fig. 8. Frequency-wavenumber (f-k) plots of the synthetic gather shown in Figs. 7a through 7c.

amplitude event (Event A) at around 0.5 sec. entirely disappeared, and that uncanceled events (Event B and C) remained. We emphasize that difference images of the truncation artifact are not due to seismic modeling or processing artifacts and cannot be removed, even if the spatial sampling is very dense, whereas the artifact due to data space aliasing can be resolved by satisfying the Nyquist sampling criterion.

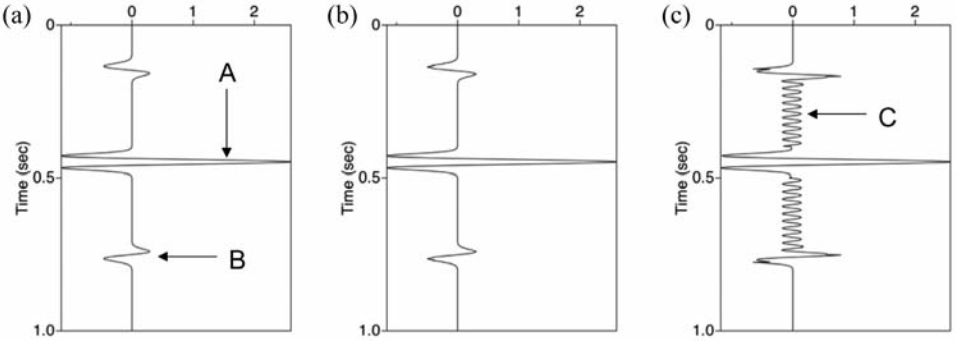

Fig. 9. Stacked traces generated from summing the synthetic gather horizontally with three different spatial sampling intervals: (a) 5 m, (b) 20 m, and (c) 80 m.

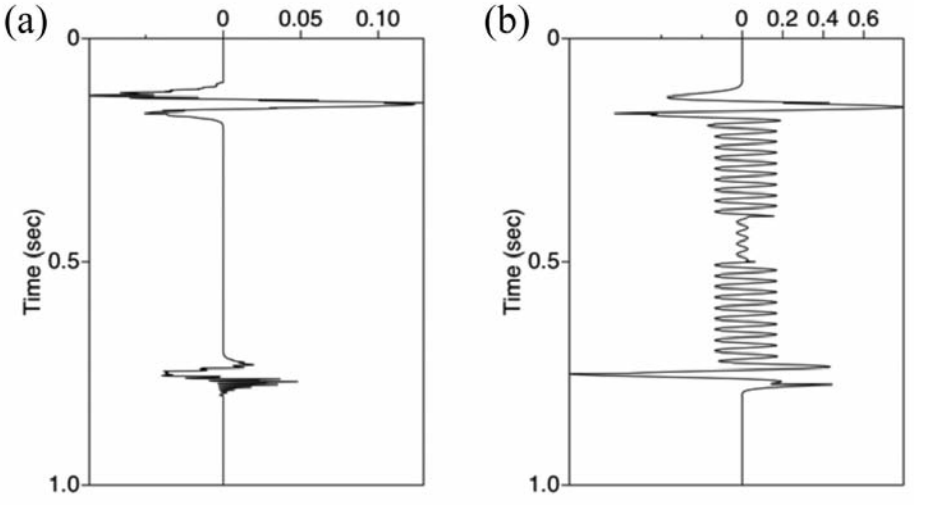

Fig. 10. Difference of two different stacked traces obtained by simple subtraction of (a) Fig. 9a from Fig. 9b, and of (b) Fig. 9a from Fig. 9c.

b. *NMO-stretch effect*

Waveform distortion due to Normal moveout (NMO) stretch is another factor for the small difference in the difference images. The stretch effect in the waveform appears as a lowering of frequency and a reduction in amplitude. We performed numerical experiments to study the effect of NMO stretch. A numerical simulation model and data acquisition geometry are shown in Fig. 11a. A source-receiver interval of width 5 m was employed, requiring 401 sources and receivers. The diffracted waves generated by a point scatterer were produced using the ray-based method. Geometrical spreading is neglected in this calculation. Thus, the amplitude of each diffracted wave is constant (= 1).

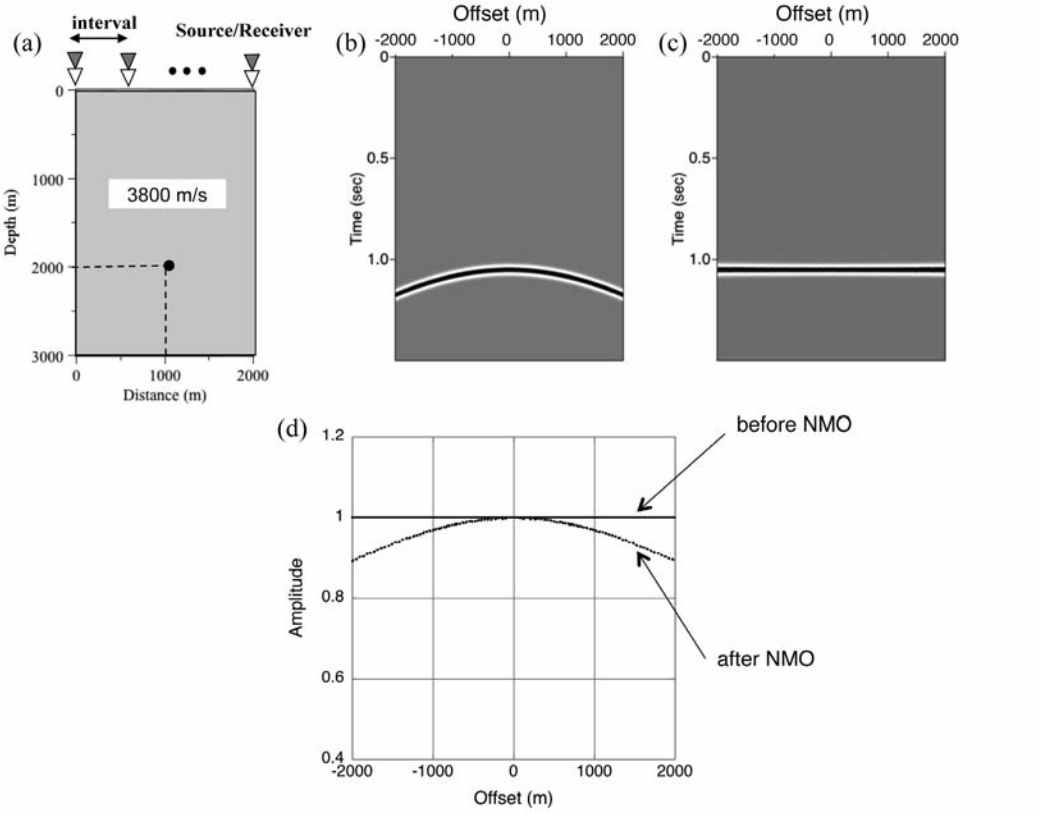

Fig. 11. (a) A single-scatterer model for numerical simulation. A scatterer is placed at a depth of 2000 m and at the center of horizontal direction. CMP gathers at the center of numerical model: (b) before NMO, and (c) after NMO correction. (d) Variation of maximum amplitude with offset for Fig. 11b (before NMO correction) and Fig. 11c (after NMO correction).

Fig. 11b shows the CMP gather at the center of numerical model. Fig. 11c shows the CMP gather after NMO correction to the CMP gathers shown in Fig. 11b. Fig. 11d shows the variation of the maximum amplitude of diffracted waves in both Fig. 11b and 11c. In Fig. 11d we can see that the maximum amplitude of Fig. 11b (before NMO correction) is constant while the maximum amplitude of Fig. 11c (after NMO correction) meets its peak at the offset of 0 m (no effect of NMO stretch) and decreases with increasing or decreasing offset. Thus, different spatial sampling causes different NMO stretch effect, resulting in small but significant differences between CMP sections (finally between migrated sections).

DISCUSSION

In random heterogeneous media, poststack migration was applied to examine different responses to different sampling intervals. Data process without data space aliasing achieves very similar final sections for different sampling intervals. Safar (1985) studied the effects of spatial sampling on the lateral resolution of a surface seismic reflection survey when carrying out scatterer point imaging by applying migration, and found almost no effect of spatial sampling on lateral resolution. Safar (1985) also demonstrated the generation of migration noise caused by a large sampling interval. Migration noise is a consequence of spatial aliasing that is related to frequency, velocity, and dip of a seismic event. A shorter sampling interval cannot improve spatial resolution very much, even if there is no noise. The same conclusion was obtained by Vermeer (1999). The results we have described above correlate well with those of these previous studies.

However, we found the existence of a small but significant difference between two images generated with adequate sampling. We examined by numerical experiments two possible reasons for this small difference: truncation artifact and NMO-stretch effect. The truncation artifact is related to a finite number of traces. Such a truncation error cannot be practically prevented, whereas the discretization error due to coarse spatial sampling can be removed by satisfying the Nyquist sampling criterion. On the other hand, NMO-stretch effect is an expression of the limited accuracy of seismic events recorded at offsets that are large relative to the reflector depth (Brouwer, 2002). Buchholtz (1972) first pointed out that the application of conventional NMO correction in the processing of seismic reflection data generates loss of frequency content and wavelet distortion due to stretch for far-offset data. Dunkin and Levin (1973) investigate in detail the effect of NMO on a seismic record. There have been many attempts to suggest alternative NMO correction methods that reduce the stretch effect (Rupert and Chun, 1975; Barnes, 1992; Perroud and Tygel, 2004). Although alternative NMO-correction methods may suffer less from stretch effects, they cannot solve completely the problem.

Our numerical studies also show that these small differences are dependent on the characteristic heterogeneity size; that is, the frequencies become lower with an increase in the characteristic size of heterogeneity. This is because the scattering effect is dominant at wavelengths comparable to the scale length of heterogeneity. The frequencies of numerous small segments produced from scattered wave fields are attributed to differences in the size of the heterogeneities. Thus, another possible direction of this kind of research is to estimate the characteristic size of heterogeneities by comparing several images with different densities of spatial sampling. Theoretically, spatial sampling should be sufficiently small to satisfy the Nyquist sampling criterion. According to the Nyquist sampling criterion, it is redundant to deploy a smaller sampling interval than the Nyquist sampling interval. However, the present numerical investigations show the practical usefulness of utilizing a highly dense deployment of source/receivers when actually applying seismic reflection methods. Further investigation is needed to quantify the characteristic size of heterogeneities. It will be helpful to analyze the amplitude and phase fluctuations of scattered seismic events occurred in difference images. Seismic scattering attenuation is another important quantity in order to characterize heterogeneities. Shapiro and Kneib (1993) clarified the nature of seismic attenuation estimations in the presence of scattering and showed its usefulness to yield statistical information of heterogeneities from seismic data.

Matsushima and Nishizawa (2010) investigated the effect of this small difference on time-lapse seismic monitoring to conclude that this difference causes numerous complicated events over the whole section in heterogeneous media even when the interval of spatial sampling becomes shorter than the Nyquist sampling interval and degrades seismic difference sections if the spatial sampling interval of base survey is not identical to that of monitor survey. Time-lapse analysis assumes implicitly that seismic surveys are repeatable, that is, the seismic response changes in time due only to changes in dynamic physical properties from subsurface. Although several successful case histories were reported in the last decade several problems remain in time-lapse analysis, mostly related to approximating the hypotheses mentioned above (Vesnaver et al., 2003). Thus, differences between seismic data sets due to other factors such as variations in acquisition/processing parameters, near-surface conditions, and background noise, must be removed or equalized prior to differencing. The cross-equalization technique (Ross et al., 1997) minimizes differences from acquisition and processing changes which increase repeatability to partially compensate for the imperfect situation.

CONCLUSIONS

We have shown from the viewpoint of spatial sampling how noise-like wave fields produced from random isotropic heterogeneity influence the seismic

section. We used a 2D finite difference method for numerically modeling acoustic wave propagation. In our numerical experiments, two different heterogeneity sizes with three different spatial sampling intervals were applied and compared, which led to the following conclusions:

- Highly dense spatial sampling does not seem to improve the final quality of a section regardless of the relationship between the spatial sampling interval and the characteristic size of heterogeneities, even when the interval of spatial sampling is smaller than the Nyquist interval. However, a small but significant difference between two sections generated with different dense samplings exists. This difference is attributed to the truncation artifact and NMO-stretch effect, which cannot be practically prevented in data acquisition.

- The difference images are dependent on the characteristic heterogeneity size, which indicates the possibility of adopting a highly dense deployment of source/receivers and differentiating two images to estimate the characteristic size of heterogeneities.

REFERENCES

Abma, R., Sun, J. and Bernitsas, N., 1999. Antialiasing methods in Kirchhoff migration. Geophysics, 64: 1783-1792.

Aki, K. and Richards, P.G., 1980. Quantitative Seismology. W.H. Freeman and Company, San Francisco.

Barnes, A.E., 1992. Another look at NMO stretch. Geophysics, 57: 749-751.

Biondi, B., 1998. Kirchhoff imaging beyond aliasing. Stanford Exploration Project, Report 97: 13-35.

Biondi, B., 2001. Kirchhoff imaging beyond imaging. Geophysics, 66: 654-666.

Brouwer, J.H., 2002. Improved NMO correction with a specific application to shallow-seismic data. Geophys. Prosp., 50: 225-237.

Brown, L., Serpa, L., Setzer, T., Oliver, J., Kaufman, S., Lillie, R., Steiner, D. and Steeples, W.D., 1983. Geology, 11: 25-30.

Buchholtz, H., 1972. A note on signal distortion due to dynamic NMO corrections. Geophys. Prosp., 20: 395-402.

Dunkin, J.W. and Levin, F.K., 1973. Effect of normal moveout on a seismic pulse. Geophysics, 28: 635-642.

Emmerich, H., Zwielich, J. and Muller, G., 1993. Migration of synthetic seismograms for crustal structures with random heterogeneities. Geophys. J. Internat., 113: 225-238.

Frankel, A. and Clayton, R., 1986. Finite difference simulations of seismic scattering. Implications for the propagation of short-period seismic waves in the crust and models of crustal heterogeneity. J. Geophys. Res., 91: 6465-6489.

Gibson, S.B. and Levander, R.A., 1988. Modeling and processing of scattered waves in seismic reflection surveys. Geophysics, 53: 466-478.

Gibson, S.B. and Levander, R.A., 1990. Apparent layering in common-midpoint stacked images of two-dimensionally heterogeneous targets. Geophysics, 53: 466-478.

Goff, J.A. and Holliger, K., 2000. Nature and origin of upper crustal seismic velocity fluctuations and associated scaling properties: Combined stochastic analyses of KTB velocity and lithology logs. J. Geophys. Res., 104: 13169-13182.

Grasmueck, M., Weger, R. and Horstmeyer, H., 2005. Full-resolution 3D GPR imaging. Geophysics, 70: K12-K19.

Hoshiba, M., 2000. Large fluctuation of wave amplitude produced by small fluctuation of velocity structure. Phys. Earth Planet. Inter., 120: 201-217.

Karson, J.A., Collins, J.A. and Casey, J.F., 1984. Geologic and seismic velocity structure of the crust/mantle transition in the Bay of Island ophiolite complex. J. Geophys. Res., 89: 3153-3171.

Maresh, J., White, R.S., Hobbs, R.W. and Smallwood, J.R., 2006. Seismic attenuation of Atlantic margin basalts: Observations and modeling. Geophysics, 71: B211-B221.

Matsushima, J., Rokugawa, S., Yokota, T., Miyazaki, T. and Kato, Y., 1998. On the relation between the stacking process and the resolution of a stacked section in a crosswell seismic survey. Explor. Geophys., 29: 499-505.

Matsushima, J., Okubo, Y., Rokugawa, S., Yokota, T., Tanaka, K., Tsuchiya, T. and Narita, N., 2003. Seismic reflector imaging by prestack time migration in the Kakkonda geothermal field, Japan. Geothermics, 32: 79-99.

Matsushima, J. and Nishizawa, O., 2010. Effect of spatial sampling on time-lapse seismic monitoring in random heterogeneous media. In: Kasahara, J., Korneev, V. and Zhdanov, M. (Eds.), Active Geophysical Monitoring, Vol 40, Handbook of Geophysical Exploration: Seismic Exploration. Elsevier Science Publishers, Amsterdam: 397-420.

Müller, T.M., Shapiro, S.A. and Sick, C.M.A., 2002. Most probable ballistic waves in random media: a weak-fluctuation approximation and numerical results. Waves Random Media, 12: 223-245.

Nishizawa, O., Satoh, T., Lei, X. and Kuwahara, Y., 1997. Laboratory studies of seismic wave propagation in inhomogeneous media using a laser Doppler vibrometer. Bull. Seismol. Soc. Am., 87: 809-823.

Perroud, H. and Tygel, M., 2004. Nonstretch NMO. Geophysics, 69: 599-607.

Ross, C.P. and Altan, M.S., 1997. Time-lapse seismic monitoring: Some shortcomings in nonuniform processing. The Leading Edge, 16: 931-937.

Rupert, G.B. and Chun, J.H., 1975. The block move sum normal moveout correction. Geophysics, 40: 17-24.

Safar, M.H., 1985. On the lateral resolution achieved by Kirchhoff migration. Geophysics, 50: 1091-1099.

Saito, T., Sato, H., Fehler, M. and Ohtake, M., 2003. Simulating the envelope of scalar waves in 2D random media having power-law spectra of velocity fluctuation. Bull. Seismol. Soc. Am., 93: 240-252.

Sato, H. and Fehler, M., 1998. Seismic Wave Propagation and Scattering in the Heterogeneous Earth. Springer-Verlag, New York.

Shapiro, S.A. and Kneib, G., 1993. Seismic attenuation by scattering: theory and numerical results. Geophys. J. Internat., 114: 373-391.

Shiomi, K., Sato, H. and Ohtake, M., 1997. Broad-band power-law spectra of well-log data in Japan. Geophys. J. Internat., 130: 57-64.

Sick, C.M.A., Müller, T.M., Shapiro, S.A. and Buske, S., 2003. Amplitude corrections for randomly distributed heterogeneities above a target reflector. Geophysics, 68: 1497-1502.

Sivaji, C., Nishizawa, O. and Fukushima, Y., 2001. Relationship between fluctuations of arrival time and energy of seismic waves and scale length of heterogeneity: an inference from experimental study. Bull. Seismol. Soc. Am., 91: 292-303.

Spitz, S., 1991. Seismic trace interpolation in the F-X domain. Geophysics, 56: 785-794.

Stolt, R., 1978. Migration by Fourier transform. Geophysics, 43: 23-48.

Vermeer, G.J.O., 1990. Seismic Wavefield Sampling. Geophysical Reference Series, Vol. 4. SEG, Tulsa, OK.

Vermeer, G.J.O., 1999. Factors affecting spatial resolution. Geophysics, 64: 942-953.

Vesnaver, A.L., Accaino, F., Böhm, G., Madrussani, G., Pajchel, J., Rossi, G. and Moro, G.D., 2003. Time-lapse tomography. Geophysics, 68: 815-823.